

Effect of Coupling Stiffness on New High-Speed Electric Machine Driveline

Juuso Narsakka, Tuhin Choudhury,
Jussi Sopanen
Department of Mechanical Engineering
LUT School of Energy Systems
LUT University
Lappeenranta, Finland
juuso.narsakka@lut.fi

Emil Kurvinen
Materials and Mechanical Engineering
Department of Mechanical Engineering
University of Oulu
Oulu, Finland
emil.kurvinen@oulu.fi

Juha Pyrhönen
Department of Electrical Engineering
LUT School of Energy Systems
LUT University
Lappeenranta, Finland
juha.pyrhonen@lut.fi

Abstract—This research studies the viability of producing a modular megawatt-class high-speed electrical machine drive that can be used in various applications, such as compressors and turbines. Currently, most high-speed drives use a standard-speed electric machine with a step-up gearbox to power a stand-alone high-speed compressor or turbine. Although direct high-speed machines are optimal for such applications, they are often not used due to their time-consuming development process and high machine cost. The long development time is due to multidisciplinary design, where even small changes in upscaling the design can cause the whole machine to be redesigned. A new high-speed drive configuration is presented to make electric machines less sensitive to system changes or application specifications. In this approach, the impeller from the application side is mounted on an additional shaft and connected to the electric motor via a flexible element. Therefore, necessary modifications can be implemented on the impeller side while the flexible element can be designed to keep the dynamics of the rotor within operational range.

Topic— *Coupling, Driveline, Electric Machine, High-speed machine, Rotordynamics*

I. INTRODUCTION

High-speed and high-power electric machines have been actively researched since the 1980s [1]. They have proven technological advantages such as high productivity and efficiency compared to traditional technologies [2]. To obtain all the benefits (oil-free, low maintenance, and footprint) of direct high-speed driveline it results in highly integrated solutions, where the application, such as a compressor or turbine, is integrated into an electric machine rotor without a gearbox (fig. 1 (a)) [3], for example, in a heat pump and Organic Rankine Cycle applications [4], [5] and [6].

The drawback of integrated solutions is the challenge of upscaling the driveline. When the machine is designed in the first place the multidisciplinary design process ends up when all the requirements from different design areas are met (In mechanical design main limitations are vibration, the strength of materials, and manufacturing). If the same design is utilized for a new application, always some changes are required, e.g., the attachment of the impeller must be tuned for the new design. When the mass and inertia of the impeller and modifications in attachment are implemented, the design easily results in a situation where one or more design requirements are not met anymore. When high-speed machines are designed near the limits redesigning leads easily to a whole new design. [7], [5], and [8].

The option for the integrated direct high-speed drive is the so-called stand-alone driveline. In stand-alone driveline electric machines and workloads are supported by their own bearings and coupled together with a flexible coupling. This enables optimization both as an individual shaft. The downside of this four-bearing driveline configuration is its requirement for two frames and the coupling. Coupling brings at least one additional axial and torsional vibration mode near the system operation area. Coupling should also withstand always some misalignment, which is in itself generating the vibration excitations [9]. If the hermetic structure is required, the coupling or the shaft requires seals, which increases the difficulty of the design.

To replace the lower efficiency [10] and oil-consuming gearbox drivelines in the future (which are still the major drivelines in volume [11], [12]) a more rapid direct high-speed drive design and utilization are needed. The utilization of the same electric machine design for the same power range

This research was conducted with the support of the Academy of Finland's Centre of Excellence in High-Speed Energy Conversion Systems. Decision number 346439. Special thanks to Toni Kangasmäki and Jouni Ryhänen for their contributions on the mechanical design, manufacturing, and assembly of driveline.

but for different applications is required. For that reason, this study proposes a new high-speed concept using a two-shaft configuration (fig. 1 (b)) which is not supported as conventional solutions with two or four radial bearings but with three of them (the third bearing is placed on extension shaft side). The rotor and an extension shaft are coupled with a flexible coupling. In the study, the feasibility of the extension shaft and the coupling concept is evaluated with the finite element method (FEM) by calculating the eigenvalues of the studied rotor geometries and verifying the results of experimental modal analysis (EMA) with a prototype rotor. The hypothesis behind the new configuration is that with the flexibility in the coupling and case-dependent extension shaft design driveline enables application-specific needs, e.g., for larger-sized impeller or wider casing of it in the way that any structural changes on the electric machine side are not required. Figure 1 (b) shows an example of extension shaft configuration in the case of a 1.5 MW direct high-speed electric machine driveline and for comparison an integrated turbine rotor configuration (a).

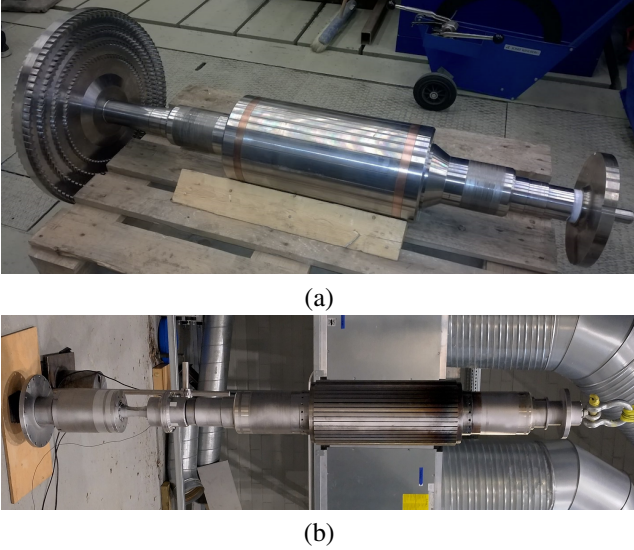


Fig. 1. (a) Rotor of 1 MW integrated high-speed steam generator. (b) 1.2 MW electric machine rotor coupled with the extension shaft and dummy impeller.

The research plan for this study follows two main steps: In the first phase, dynamic characteristics are studied by changing the stiffness properties at the coupling location in the finite element analysis (FEA) model and analyzing the natural frequency of the drive. The purpose of this parametric analysis is to find the suitable stiffness properties and consequent effects of the change in radial, axial, and torsional direc-

tions. The second step includes the analysis of a commercial flexible coupling commonly used in high-speed drives. This step demarcates the manufacturability of required flexibility in the coupling and shows its strengths and weaknesses. To compare suitable stiffness properties and commercial coupling driveline, their stiffness characteristics must be evaluated. To validate the simulation model experimental modal analyses are performed. Once the simulation model is validated, the effects of changes in the driveline are studied by changing the geometrical properties of the workload. To benchmark the results and confirm the hypothesis, the integrated driveline is analyzed alongside the extension shaft.

II. ANALYSIS OF EXTENSION SHAFT DRIVELINE CONFIGURATION

Methods section includes the method to assess the effect of coupling flexibility in the extension shaft driveline. It introduces briefly how the spring-damper values can be analyzed using a solid element model and experimental measurements. And it presents how the geometrical changes related to the impeller mass properties and installation are varied in the driveline.

A. Effect of coupling flexibility on the dynamics of the driveline

A beam element-based rotor system model is used for computationally efficient analysis. A low degree of freedom model is particularly important in further AMB control analysis. Widely utilized beam element formulation based on Timoshenko beam theory is proven to provide reasonably accurate results and is applied at the design phase in rotor dynamic analysis [13], [14]. The equation of motion to solve speed-dependent natural frequencies is written as:

$$\mathbf{M}\ddot{\mathbf{x}}(t) + (\mathbf{C} + \Omega\mathbf{G})\dot{\mathbf{x}}(t) + \mathbf{K}\mathbf{x}(t) = \mathbf{F}(t), \quad (1)$$

where \mathbf{M} , \mathbf{C} , \mathbf{G} and \mathbf{K} are the mass, damping, gyroscopic, and stiffness matrices of the rotating system, \mathbf{F} represents the general external forces, for example, due to unbalance, gravity, or other external excitations. These matrices are defined using the finite element model of the rotor-bearing system. The stiffness matrix \mathbf{K} includes the stiffness of the rotor and the bearing coefficients at the respective node location. Similarly, the damping matrix \mathbf{C} includes the non-rotating internal damping of the rotor and the bearing damping coefficients. $\ddot{\mathbf{x}}$, $\dot{\mathbf{x}}$, \mathbf{x} represent the acceleration, velocity and displacement

vectors respectively and Ω represents the rotational speed. To solve natural frequencies and mode shapes a state space representation is utilized. Equation of motion (eq. 1) in state space form can be written as:

$$\dot{\mathbf{y}} = \mathbf{A}\mathbf{x} + \mathbf{B}\mathbf{u}, \text{ where,} \quad (2)$$

$$\mathbf{A} = \begin{bmatrix} \mathbf{0} & \mathbf{I} \\ -\mathbf{M}^{-1}(\mathbf{K} + \mathbf{K}_{\text{amb}}) & -\mathbf{M}^{-1}(\mathbf{C} + \mathbf{G}\Omega) \end{bmatrix},$$

$$\text{and, } \mathbf{B} = \begin{bmatrix} \mathbf{0} \\ \mathbf{M}^{-1}\mathbf{F} \end{bmatrix},$$

where \mathbf{K}_{amb} presents the AMB support stiffness matrix. Natural frequencies (eigenvalues) and mode shapes (eigenvectors) can be solved from the state space matrix \mathbf{A} [15]. When driveline free-free frequencies and mode shapes are solved terms \mathbf{K}_{amb} and Ω are zeros, meaning that there is no bearing support or gyroscopic effect on the calculation. In general free-free modes are calculated for model validation purposes. Experimental tests for operational frequencies require the whole machine in operational condition.

Cavalca et al. [16] have proposed how flexible elements can be simply represented by a spring-damper arrangement and how the stiffness and damping matrices can be derived. With the spring-damper, the stiffness at coupling values can be rapidly varied. These variations can be analyzed to determine how a possible flexible element affects the overall dynamics of the driveline. To illustrate the concept of flexibility, free-free analysis is used. It should be noted that free-free frequencies can be significantly lower than critical speeds, so free-free results cannot be used to directly assess the operation range of different stiffness values. Directional stiffness (radial in two plane and axial) values in the coupling are varied between $1 \cdot 10^3 - 1 \cdot 10^{11}$ N/m. Rotational or angular stiffness around all axes (bending around two radial axes and torsion) is varied with the same magnitude, even though it has a different unit of Nm/rad. Figure 2 shows the beam element model investigated in the study. The spring-damper element is located between nodes 45 and 46 and it represents the stack of thin discs present in the physical coupling. A rotor-bearing dynamic tool (RoBeDyn) developed at LUT University is used to compute the results. It has been used in several publications for rotor design and analysis purposes [5], [8], [17].

B. Disc coupling stiffness analysis

In this study the flexible coupling is not designed but commercial disc coupling is used for reference and to validate

the simulation model. Disc couplings are used with high-speed applications due to their capability to allow angular misalignment (low bending stiffness) but simultaneously transfer a high torque [18]. The specific coupling in this study contains only one flexible element (one set of thin laminated discs), whereas normally disc couplings are used in pairs (which also allows parallel misalignment between the shafts). Fig. 2 also shows the 3D model of the disc coupling used in this study.

Only torsional stiffness was provided by the manufacturer. In the literature, there are methods to evaluate disc coupling stiffness values, although most of the studies are focused on torsional stiffness [19]. In this study, the natural frequencies of the whole driveline are first obtained from a detailed solid element model of the driveline using ANSYS 2021 R2 software. Then, the results of solid element model are used to tune the spring-damper coefficients of coupling in a beam element model so that the first two bending modes as well as the lowest axial and torsional modes match the solid element model. Finally, driveline's natural frequencies and modes are measured with a scanning laser doppler vibrometer (Polytec PSV-500) and results from the experimental modal analysis are used to verify the simulation results. Figure 1 (b) illustrates how the driveline was placed in the measurements.

C. Evaluation of coupling driveline dynamic characteristics under geometrical variation

The electric machine rotor used in this study is designed for multi-megawatt high-speed operation [8]. The original rotor contains three RAMBs on the same shaft. The rotor is then rebuilt with two RAMBs. To analyse how the extension shaft configuration behaves under modification, the impeller diameter is varied from 200 mm up to 600 mm. The impeller is modeled as a point mass where its mass, polar, and diametral

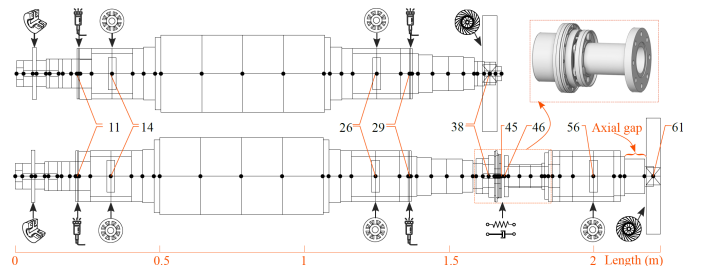


Fig. 2. The beam element models of the integrated rotor (top) and the same rotor with extension shaft design (bottom) were used in this study to investigate the effectiveness of coupling stiffness values. The figure also shows the key node locations for components such as bearings, sensors, and impellers

mass moment of inertia are varied. The width and density of the impeller are in all cases 50 mm and 7800 kg/m³, respectively.

A second variation is made with the gap between the touchdown bearings and the disc. In an integrated driveline, that gap is required for the impeller casing. It can vary from under 20 mm to over 100 mm. For example, in a 1 MW two-sided axial turbine disc, the casing requires 100 mm of space [6]. In a variation of the gap, the impeller parameters are kept constant and vise-versa. In all parametric analyses the coupling parameters are kept constant. For comparison of extension shaft results, the same rotor is analyzed in an arrangement where the impeller is attached to the end of the rotor (integrated drive). The impeller is inserted into rotor node number 38 (Fig. 2) and all elements from 38 above were left out of the model.

III. RESULTS OF THE STUDY

The results section has three parts. The first part shows how the flexibility of the coupling affects the natural frequencies of the driveline. The second part compares the outputs from FEM simulations with the experimental measurements using disc coupling. The final subsection shows the results of variations in impeller diameter and the required gap of impeller casing.

A. Effect of the flexible element in the driveline

The analysis starts with the variation of radial and bending stiffnesses of the coupling. Stiffnesses in both radial directions are set to the same value, and bending values are treated similarly. Figure 3 presents the free-free natural frequencies in variations of the radial and bending stiffnesses in the coupling. Typical operation speed range for megawatt range electric machine is highlighted in the figures [8], [12]. Only one value of radial, bending, axial, or torsional is varied at the time, other values are kept at $1 \cdot 10^3$ in the analysis. In radial (a) and bending (b) cases it must be noted that the limiting critical speed is usually higher than free-free frequencies when AMBs are used (can be seen from fig. 5). Figure 4 illustrates how the mode shapes change when stiffness values are changed between $1 \cdot 10^6$ (a, c) and $1 \cdot 10^8$ (b, d) in both bending (Nm/rad) and radial (N/m) cases. The first two rows of Fig. 4((a), (b)) shows how the rotor and extension shaft behaves almost as rigid bodies, and bending is happening over the coupling with both stiffness values. This mode is called a coupling-bending mode. In the third row in Fig. 4(c), with the value of $1 \cdot 10^6$,

the rotor behaves mainly as a rigid body. However, with the stiffness value of $1 \cdot 10^8$ (d), the mode shape of the drive is clearly uniform and both the rotor and shaft behave as flexible bodies. This mode is called a coupling-radial mode.

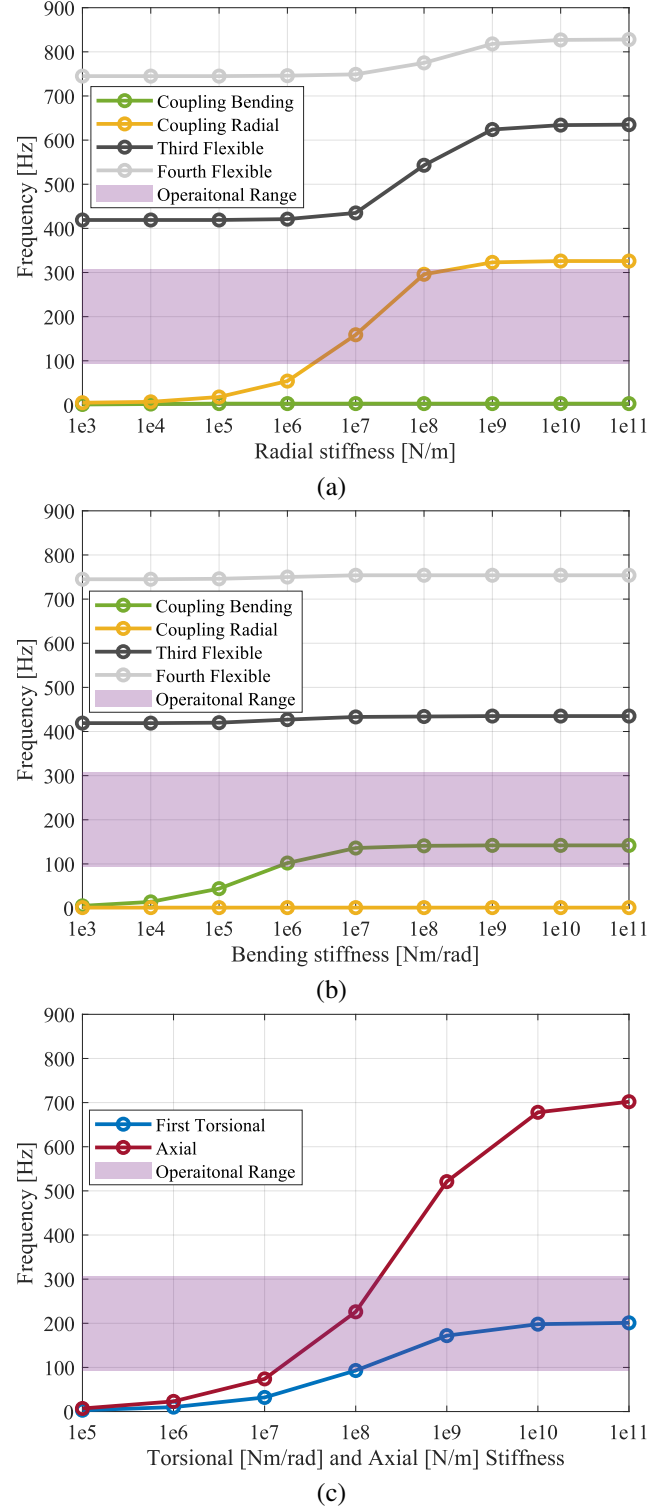


Fig. 3. Effect of (a) radial and (b) bending (c) torsional and axial stiffness variation on the natural frequencies (free-free) of the drive-train case study.

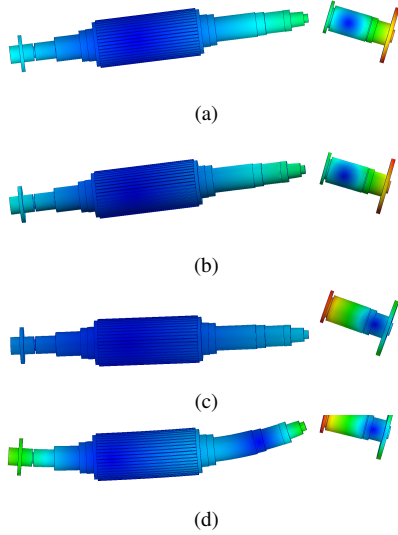


Fig. 4. Mode shapes when stiffness is at the level of $1 \cdot 10^6$ (a and c) and $1 \cdot 10^8$ (b and d). The first two line (a and b) presents the coupling-bending mode and the last two lines (c and d) the coupling-radial mode.

Next, the axial and torsional stiffnesses were varied, and the results can be seen in Fig. 3 (c). The torsional mode shape deflects with low torsional stiffness mostly over the coupling location. When rotational stiffness is increased, the whole drive line is deflected. The axial mode shape behaves similarly, with the low stiffness in axial direction deformation appear locally in the coupling location and with the high value uniformly.

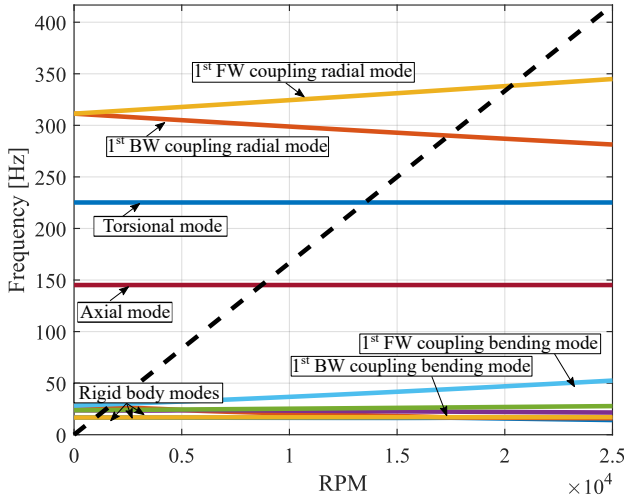


Fig. 5. Campbell diagram of the disc coupling driveline.

B. Comparison of disc coupling driveline experimental results and simulation

Table I presents the first four analysed and measured natural frequencies of the driveline where mode shapes deflect in

a radial direction (i.e., shaft bending modes) and first axial and torsional modes. Stiffness coefficients of the beam model spring-damper are for; bending $6.6 \cdot 10^4$ Nm/rad, radial $3.6 \cdot 10^8$ N/m, axial $5.0 \cdot 10^7$ N/m, torsional $2.8 \cdot 10^6$ Nm/rad.

TABLE I. Comparison of measured and simulated results of driveline with spring-damper beam element model (SDBEM) and solid element model (ANSYS).

Mode	ANSYS [Hz]	SDBEM [Hz]	Measured [Hz]
1 st flexible (coupling-bending)	22	22	8.5
2 nd flexible (coupling-radial)	327	311	301
3 rd flexible (banana-shape for both)	596	596	517
4 th flexible *	830	795	678
1 st axial mode	146	146	166
1 st torsional mode	225	225	235

* Rotor in s-shape, ext. shaft in a banana

Figure 6 presents coupling-bending and coupling-radial modes from measurements and beam model simulations. The amplitude of the vibration is normalized in both cases. The mode shapes are overlapped with the driveline beam model.

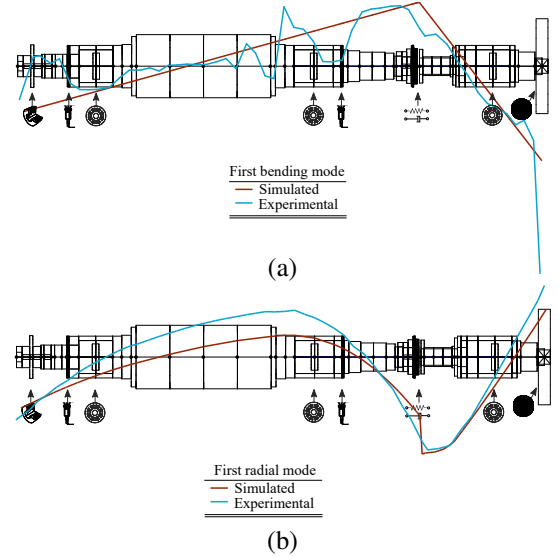


Fig. 6. (a) The simulated (brown line) and experimentally tested (blue line) mode shapes of the coupling-bending mode. (b) The simulated and experimentally tested mode shapes of the coupling-radial mode. The amplitudes of the modes are normalized.

All the results presented so far are the drive's natural frequencies at zero speed and in free-free boundary conditions, i.e., without the bearings and support. In the case of AMBs, bearing stiffness is so low that it does not affect the zero-speed results significantly. The effect of bearing stiffness can be seen when the results from the table I (beam element) are compared to the results of the Campbell diagram at zero speed (Fig. 5). The stiffness value for the bearing is set to be 2 MN/m. The Campbell diagram shows the rotational velocity's effect on

the driveline's natural frequencies. The yellow line in Fig. 5 shows the forward mode of coupling-radial mode, which can be considered as a limiting factor for maximum operational speed. Rigid, axial, torsional, and coupling-bending modes are considered to be able to cross.

C. Effect of change in impeller mass properties and dimensions on natural frequencies of driveline

Figure 7 (b) and (c) shows how the variations in impeller mass properties and dimensions affect the 1st Forward Whirling (FW) critical speeds of the driveline. The outer diameter (OD) of the impeller was varied first, which also changes the impeller mass properties as illustrated in 7 (a). Firstly, the results were obtained for the extension shaft configuration. The lowest frequencies resulted from an impeller OD of 300 - 400 mm (284 Hz). The overall difference between the different impeller ODs was at a maximum of 20 Hz, which is a 6.6% deviation from the highest value (304 Hz). Next has performed the gap length variation. The initial gap used in disc variation was 50 mm. The disc OD in the gap variation was selected to be 400 mm. As can be seen from Fig. 7 (b) by increasing the gap length the critical speed will decrease. The effect of change decreases a little when the gap length increases but it is near the linear value of 0.45 Hz/mm over the range. The third step was to analyze integrated drive results with the same variation. After the variation effect of disc diameter change was resulted to be 26.2% at maximum. The effect of gap variation resulted in being approximately 0.75 Hz/mm.

IV. DISCUSSION

The purpose of the study was to find out if there is a possibility to separate the electric machine and workload in such a way that rotor dynamics are independent of the workload. The results (Fig. 3) show that, with the low stiffness of the coupling, rotor and extension-shaft dynamic coupling are minor. The vibration behavior matches the cases where both the rotor and extension shaft act as individual components (Fig. 4 (a,c)). With the low stiffness values, the workload could be designed with a minor effect on the electric machine. However, there is a possible problem with large deformation over the coupling in an overhung structure when the radial stiffness is low, causing the angular misalignment and thus excessive vibration. If future studies with the AMB control model result in the need for high radial stiffness, it is best to design it as high as possible. With a combination of low bending stiffness

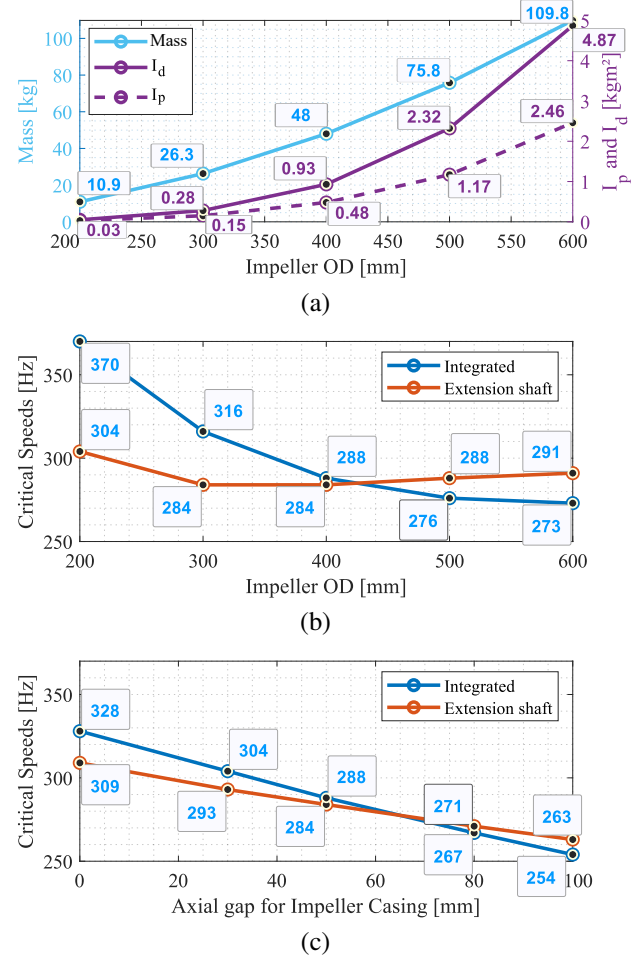


Fig. 7. (a) The mass, polar, and diametral mass moment of inertia of the impeller when the outer diameter is varied. (b) Effect of the same variation in impeller size on 1st FW critical speed (For the extension-shaft case, it is the radial coupling mode.) (c) Effect of variation in the axial gap for impeller casing (Hz) on the same mode.

and high radial stiffness, an operational range can be designed between the coupling-bending and -radial modes (as can be seen from the disc coupling case). Even with a combination of high radial and low bending stiffnesses, changes in workload had a minor effect on the critical speed of the driveline. The difference in mode shapes over the geometrical variation was not investigated, and some effects from the controllability side can still be found. However, the insensitivity to changes in workload provides a promising foundation for the utilization of the extension shaft configuration.

In the beam element model used for analyzing the flexibility and geometrical variation, the spring-damper for the flexible element was utilized. For verification purposes, the disc coupling driveline was experimentally analyzed. From Table I can be seen that the coupling-radial mode could not be matched

exactly with the solid element model (the model could not reach the frequency level in any radial stiffness value). Rather than matching the coupling-radial mode frequency, matching was done with the third bending mode frequency. So, from the radial stiffness values, an exact value cannot be determined with high accuracy by comparing the solid and beam element models, but one can say that the stiffness in the flexible element is at the same level as the structure stiffness on both sides of the coupling. Coupling-bending mode was able to match the simulation models. However, the same frequency could not be found through experimental analysis. The frequency at which these modes appear similarly was found at a much lower level. The experimentally obtained mode shape of coupling-bending mode does not appear clearly from the measurements and cannot be concluded to be exactly the same mode. Although no experimental verification was obtained with the coupling-bending mode in this study, it can be stated that the simulation model produces results in sufficient accuracy for the scope of this work.

V. CONCLUSIONS

In the study, a driveline with three radial AMBs, two shafts, and flexible coupling is proposed and investigated. The main focus is determining the influence of coupling stiffness on the rotor dynamics. The results indicate that the coupling with the optimized stiffness values can be designed, and it provides the extension shaft configuration a wider operation range than the corresponding integrated machine with heavier workloads. In future studies, different coupling configurations can be designed and analyzed. Additional studies can include the design and optimization of the extension shaft assembly, which includes the shaft, impeller, and radial and axial magnetic bearings. The extension for this study is planned to design the radial AMB control model to investigate how different stiffness coefficients in the coupling and loads affect the behavior. In the case of disc coupling in the driveline, more analysis and experimental tests are required for accurate results and design decisions.

REFERENCES

- [1] J. Larjola, A. Arkkio, and J. Pyrhönen, "Suurnopeustekniikka-high speed technology in finland," *Yliopistopaino*, 2010.
- [2] R. R. Moghaddam, "High speed operation of electrical machines, a review on technology, benefits and challenges," in *2014 IEEE Energy Conversion Congress and Exposition (ECCE)*. IEEE, 2014, pp. 5539–5546.
- [3] R. Abebe, M. Di Nardo, D. Gerada, G. L. Calzo, L. Papini, and C. Gerada, "High speed drives review: Machines, converters and applications," in *IECON 2016-42nd Annual Conference of the IEEE Industrial Electronics Society*. IEEE, 2016, pp. 1675–1679.
- [4] R. P. Jastrzebski, D. Kepsu, A. Putkonen, I. Martikainen, A. Zhuravlev, and S. Madanzadeh, "Competitive technology analysis of a double stage kinetic compressor for 0.5 mw heat pumps for industrial and residential heating," in *2021 IEEE International Electric Machines & Drives Conference (IEMDC)*. IEEE, 2021, pp. 1–7.
- [5] D. Kepsu, E. Kurvinen, J. Tiainen, J. Honkatukia, T. Turunen-Saaresti, and R. P. Jastrzebski, "Interdisciplinary design of a high-speed drivetrain for a kinetic compressor in a high-temperature heat pump," *IEEE Access*, vol. 9, pp. 143 877–143 900, 2021.
- [6] A. Grönman, J. Nerg, E. Sikanen, T. Sillanpää, N. Nevaranta, E. Scherman, A. Uusitalo, N. Uzhegov, A. Smirnov, J. Honkatukia *et al.*, "Design and verification of a hermetic high-speed turbogenerator concept for biomass and waste heat recovery applications," *Energy Conversion and Management*, vol. 225, p. 113427, 2020.
- [7] N. Uzhegov, E. Kurvinen, J. Nerg, J. Pyrhönen, J. T. Sopanen, and S. Shirinskii, "Multidisciplinary design process of a 6-slot 2-pole high-speed permanent-magnet synchronous machine," *IEEE Transactions on Industrial Electronics*, vol. 63, no. 2, pp. 784–795, 2015.
- [8] E. Kurvinen, C. Di, I. Petrov, J. Nerg, O. Liukkonen, R. P. Jastrzebski, D. Kepsu, P. Jaatinen, L. Aarniovuori, E. Sikanen *et al.*, "Design and manufacturing of a modular low-voltage multimegawatt high-speed solid-rotor induction motor," *IEEE Trans. on Ind. App.*, vol. 57, no. 6, pp. 6903–6912, 2021.
- [9] F. W. da Silva Tuckmantel and K. L. Cavalca, "Vibration signatures of a rotor-coupling-bearing system under angular misalignment," *Mechanism and Machine Theory*, vol. 133, pp. 559–583, 2019.
- [10] K. Vostrov, L. Aarniovuori, and J. Pyrhönen, "High-speed megawatt-scale induction-motor drives: Efficiency maps and drivetrains," in *2022 International Conference on Electrical Machines (ICEM)*. IEEE, 2022, pp. 745–751.
- [11] Global Industry Analysts Inc, "Industrial gearbox - global market trajectory & analytics," p. 713, Sep. 2020.
- [12] Global Industry Analysts Inc., "Global industrial solution high-speed motor industry market research report," p. 144, May 2020.
- [13] J. Rao, "Finite element methods for rotor dynamics," in *History of Rotating Machinery Dynamics*. Springer, 2011, pp. 269–297.
- [14] D. L. Logan, *A first course in the finite element method*. Cengage Learning, 2016.
- [15] D. J. Inman, *Engineering vibration*, 3rd ed. Upper Saddle River (NJ): Pearson Prentice Hall, 2008.
- [16] K. Cavalca, P. Cavalcante, and E. Okabe, "An investigation on the influence of the supporting structure on the dynamics of the rotor system," *Mechanical Systems and Signal Processing*, vol. 19, no. 1, pp. 157–174, 2005, <https://doi.org/10.1016/j.ymssp.2004.04.001>.
- [17] T. Choudhury, R. Viitala, E. Kurvinen, R. Viitala, and J. Sopanen, "Unbalance estimation for a large flexible rotor using force and displacement minimization," *Machines*, vol. 8, no. 3, p. 39, 2020.
- [18] J. P. Corcoran, D. Lyle, P. McCormack, T. Ortel *et al.*, "Advances in gas turbine couplings," in *Proceedings of the 36th Turbomachinery Symposium*. Texas A&M University. Turbomachinery Laboratories, 2007.
- [19] B. Zhao, Y. Zhao, J. Feng, and X. Peng, "Numerical and experimental investigation of the torsional stiffness of flexible disc couplings," *International Journal of Mechanical Sciences*, vol. 114, pp. 207–216, 2016.